Electrical conductance in duplex DNA: Helical effects and low-frequency vibrational coupling

Enrique Maciá
Departamento de Física de Materiales, Facultad CC. Físicas, Universidad Complutense de Madrid, E-28040 Madrid, Spain
(Received 17 October 2007; published 26 December 2007)

In this work we consider the combined effect of helical structure and base-pair twist motion on charge transfer through duplex DNA at low temperatures. We present a fully analytical treatment of charge-lattice coupled dynamics in terms of nearest-neighbor tight-binding equations describing the propagation of the charge through an effective linear lattice for certain frequency values. The corresponding effective hopping terms include both helicoidal and dynamical effects in a unified way. Although base-pair motion generally reduces π-π stack overlapping, the coupling to certain normal modes gives rise to a significant improvement of the Landauer conductance.

DOI: 10.1103/PhysRevB.76.245123 PACS number(s): 87.14.Gg, 72.80.Le, 72.20.Ee

I. INTRODUCTION

Charge migration in DNA depends on the coupling between π orbitals belonging to neighboring nucleobases stacked along the helix axis direction.[1,2] According to quantum-chemical studies on DNA oligomers, as a first approximation one can describe this charge transfer mechanism by treating each Watson-Crick base pair (bp) as a single entity with a characteristic on-site energy.[3–7] In this way, the most basic features of DNA electronic structure can be incorporated into effective model Hamiltonians describing DNA as a linear chain with a tight-binding orbital per site (each lattice site representing a bp), along with a suitably parametrized hopping onto neighboring sites. A more accurate description requires us to model each nucleobase in a bp as an independent site as well as including the sugar-phosphate backbone.[8] The hydrogen bonding between complementary bases is then described as an additional hopping term perpendicular to the DNA stack,[9–13] and appropriate on-site energies and hopping parameters for the backbone must be included as well.[14–16] The resulting models are essentially a planar projection (two dimensions) of the DNA structure with its double helix unwound, so that the successive bp's are lined up face to face along the strand. This geometrical constraint optimizes the π-π orbital coupling between neighboring bases, hence overestimating charge transport efficiency.

In physiological conditions, however, DNA double helix exhibits a full-fledged three-dimensional (3D) geometry, so that every two consecutive bases are twisted by a certain angle ($\theta_0 \simeq \pi/5$ in equilibrium conditions). As a result, the orbital overlapping is substantially reduced, yielding smaller values for the transfer integral values.[1,17] Therefore, one should expect a significant reduction of the charge transfer efficiency stemming from purely geometrical considerations (dimensionality effect). In addition, at physiological temperatures the relative orientation of neighboring bases becomes a function of time, thereby modifying their mutual overlapping in an oscillatory way (dynamical effect). The motion of bases can either occur in a synchronized manner (normal mode propagation) or incoherently (due to thermal motion). The role of thermal fluctuations on the charge transfer efficiency has been discussed in a number of recent papers where the structural fluctuations of the DNA double helix are described by sampling the initial angular velocities and twist angles from a Boltzmann distribution at a given temperature.[18–24] In this work we will focus on coherent transport due to the coupling between low-frequency vibration modes and charge motion through duplex DNA, and we will explicitly take into account its characteristic helical geometry.

II. DNA MODEL DESCRIPTION

A. Dynamical degrees of freedom

When describing the phonon dynamics in DNA one can disregard the inner degrees of freedom of the bases, since we can separate the fast vibrational motions of atoms about their equilibrium positions from the slower motions of molecular groups. At the molecular level the basic dynamical building blocks are the sugar-phosphate groups and the nucleobases. The nucleobases will be treated as identical point masses, helically arranged and mutually connected by means of elastic rods, which describe the sugar-phosphate backbone.[25–27] Adopting the reference frame indicated in Fig. 1(a), the position of the nth nucleobase can be expressed as $x_n = r_n \cos \varphi_n$, $y_n = r_n \sin \varphi_n$, and $z_n = c\varphi_n$, where n labels the considered bp along the DNA double strand, r_n and φ_n are usual cylindrical coordinates, and $c = h_0/\theta_0$, $h_0 \simeq 0.34$ nm being the equilibrium separation between two successive bp planes (B-DNA form). Thus, the Euclidean distance between two neighboring bases can be expressed as

$$d_{n,n\pm1} = \sqrt{c^2\theta_{n,n\pm1}^2 + r_n^2 + r_{n\pm1}^2 - 2r_n r_{n\pm1}\cos\theta_{n,n\pm1}}, \quad (1)$$

where $\theta_{n,n+1} \equiv \varphi_{n+1} - \varphi_n$ ($\theta_{n,n-1} \equiv \varphi_n - \varphi_{n-1}$) measure the relative angular displacement between two adjacent bp's. In equilibrium conditions (i.e., $r_n = R_0 \simeq 1$ nm, $\theta_{n,n\pm1} = \theta_0 \forall n$) Eq. (1) reduces to $l_0 = \sqrt{h_0^2 + 4R_0^2 \sin^2(\theta_0/2)} \simeq 0.7$ nm.[25–27] The arc length between two consecutive points along the helix is given by $s_{n,n+1} = \sqrt{R_0^2 + c^2}\Delta\varphi$. This value has been considered as an approximate expression for the helix arc length in a number of previous works dealing with a rigid backbone structure.[25–27] In general, the shortest path between two points (not directly above the other) on a cylinder of radius ρ is given by the arc length between two consecutive

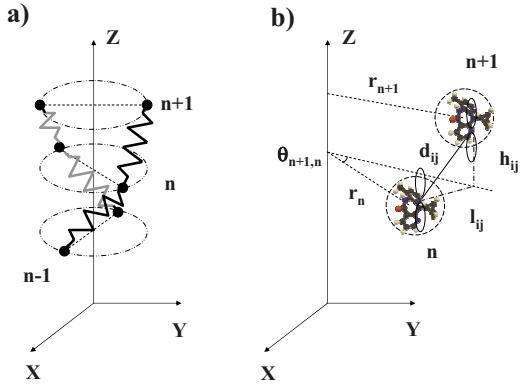

FIG. 1. (Color online) Sketch illustrating the adopted DNA model at two different scale lengths. (a) At the molecular level the corresponding dynamical degrees of freedom are described in terms of cylindrical coordinates. (b) the p_z atomic orbital overlapping between neighboring nucleobases is described in terms of Cartesian coordinates referred to the nucleobase center of mass. Its position, in turn, is determined by the relative twist and radial variables, $\theta_{n,n+1}$ and r_n at the molecular scale.

points along a helix, according to the formula

$$s_{n,n\pm1} = \int_{\varphi_n}^{\varphi_{n+1}} \sqrt{\rho^2 + c^2} d\varphi. \tag{2}$$

In the limit of small twist oscillations ($r_n = R_0$, $\theta_{n,n+1} \ll 1$) Eq. (1) reads

$$d_{n,n\pm1} = \sqrt{R_0^2 + c^2}\theta_{n,n\pm1} \equiv \xi\theta_{n,n\pm1} = s_{n,n\pm1}, \tag{3}$$

so that the Euclidean distance given by Eq. (1) coincides with the helix arc length in this case.

B. Effective Hamiltonian

The effective model Hamiltonian can be expressed as the sum of two main contributions $H = H_e + H_l$, where H_e describes the charge carrier dynamics over the π-stacked electronic system and H_l describes the duplex DNA dynamics. Following previous works, the electronic degrees of freedom of a double-stranded DNA (including sugar-phosphate and environmental effects) are described in terms of a renormalized, one-dimensional effective Hamiltonian given by[15,16]

$$H_e = \sum_{n=1}^{N} [\alpha_n(E) c_n^\dagger c_n - t_{n,n+1}(\theta_{n,n+1})(c_{n+1}^\dagger c_n + c_n^\dagger c_{n+1})], \tag{4}$$

where $c_n^\dagger$ (c_n) is the creation (annihilation) operator for a charge at nth site and N is the number of bp's. Equation (4) describes the charge carrier propagation through a DNA duplex in terms of an equivalent monatomic lattice, where the renormalized "atoms" α_n correspond to complementary pairs in the original DNA molecule, and $t_{n,n+1}(\theta_{n,n+1})$ is the transfer integral describing the aromatic base stacking between adjacent nucleotides. The renormalized on-site energies enclose substantial physicochemical information about the Watson-Crick bp energetics through the expressions[15,16]

$$\alpha(E) = \alpha_0 + \alpha_1 E + \frac{2t^2}{E - \gamma}, \quad \beta(E) = \beta_0 + \beta_1 E + \frac{2t^2}{E - \gamma}, \tag{5}$$

with $\alpha_0 \equiv a_0 - \gamma\alpha_1$, $\beta_0 \equiv b_0 - \gamma\beta_1$, $a_0 \equiv t_{GC} + 2(\varepsilon_G + \varepsilon_C)$, $b_0 \equiv t_{AT} + 2(\varepsilon_A + \varepsilon_T)$, $\alpha_1 \equiv (\varepsilon_G^2 + \varepsilon_C^2)/t^2$, and $\beta_1 \equiv (\varepsilon_A^2 + \varepsilon_T^2)/t^2$, where $t_{GC(AT)}$ describes the hydrogen bonding between the complementary bases, ε_k are the nucleobases on-site energies, t describes the transfer integral between backbone and base states, and γ accounts for the sugar-phosphate backbone on-site energies, generally depending on the presence of water molecules and counterions attached to the backbone.

Three characteristic vibrational states have been usually considered in DNA normal mode calculations, namely, the stretch oscillations of each base back and forth with respect to the center of mass of the system located at the helical axis, longitudinal oscillations of the bp planes along the helix axis, and twist oscillations of each bp as a whole around the helical axis.[25–27] In a recent work the effect of twisting on charge transport through DNA was investigated by considering two types of polarons depending on the coupling between the transfer integral and nucleotide geometry: radial polarons (where charge induced deformations mainly affect the radial variables) and twist polarons. The authors concluded that twist polarons can transport charge in a very efficient way (even in the presence of a base-pair inhomogeneity), whereas radial polarons experience either reflection or trapping.[28] Accordingly, in this work we will focus on the low-frequency twist mode, hence keeping $r_n = R_0 \forall n$.[29] In that case, considering a harmonic coupling between neighboring bases along the helical strand and making use of Eq. (1), one can express the lattice Hamiltonian in the form

$$H_l = \frac{1}{4m\xi^2}\sum_{n=1}^{N} p_{\varphi,n}^2 + k\sum_{n=1}^{N-1}\left[\sqrt{c^2\theta_{n,n+1}^2 + 4R_0^2 \sin^2\left(\frac{\theta_{n,n+1}}{2}\right)} - l_0\right]^2, \tag{6}$$

where m is the base mass, ξ is the effective helix arc length introduced in Eq. (3), $p_{\varphi,n}$ is the angular momentum, k is an effective force constant, and l_0 is the equilibrium distance.

Hamiltonians (4) and (6) describe the most relevant physics of the DNA molecule and its environment in terms of the model parameters $\alpha_n(E)$ and $t_{n,n\pm1}(\theta_{n,n\pm1})$. As it is illustrated in Fig. 1(b), the overlapping between π orbitals of stacked bp's depends on the Euclidean distance between atoms belonging to neighboring nucleobases, given by $d_{ij} = \sqrt{l_{ij}^2 + h_{ij}^2}$. Following the procedure described in Refs. 1 and 30 the transfer integral between successive bp's can be expressed in the form

$$t_{n,n\pm1}(r_n, \theta_{n,n\pm1}) = t_0[1 - \bar{\eta} l_0^{-2}(r_n^2 + r_{n\pm1}^2 - 2r_n r_{n\pm1}\cos\theta_{n,n\pm1})], \tag{7}$$

where t_0 is the transfer integral corresponding to the planar geometry and $\bar{\eta} \equiv 1 + |\eta_{pp\pi}|/\eta_{pp\sigma}$, where $\eta_{pp\pi}$ and $\eta_{pp\sigma}$ describe the hybridization matrix elements between neighboring bases p_z orbitals.[1] To obtain Eq. (7) we have assumed

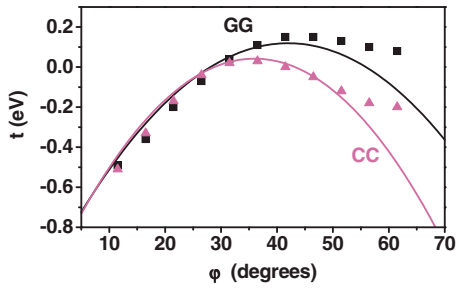

FIG. 2. (Color online) Transfer integral as a function of the twist angle between neighboring GG (squares) and CC (triangles) bases in the same strand (after Ref. 24). The solid lines are obtained from expression $t=t_{jj}[1-\chi_{jj}(\theta-\theta_{jj})^2]$ with $t_{GG}=0.119$ eV, $t_{CC}=0.042$ eV (Ref. 24), $\chi_{GG}=17$, $\chi_{CC}=63$, $\theta_{GG}=42°$, and $\theta_{CC}=36°$, respectively.

that the atomic orbitals are orthogonal to each other and the mean distances among atoms belonging to different nucleobases can be roughly approximated as $\langle d_{ij}\rangle \simeq l_0$ and $\langle l_{ij}^2\rangle = r_n^2 + r_{n\pm1}^2 - 2r_n r_{n\pm1}\cos\theta_{n,n\pm1}$. In this way, one recovers the usual expression $t_{n,n\pm1}=t_0$ for a planar model (i.e., $r_n=R_0$, $\varphi_n \equiv 0\,\forall n$). If we now allow for a full 3D description of the helix geometry (i.e., $r_n=R_0$, $\theta_{n,n\pm1}=\theta_0$), Eq. (7) takes the form

$$t_{n,n\pm1}(R_0,\theta_0) = t_0\left[1-\bar{\eta}\left(\frac{2R_0}{l_0}\sin\frac{\theta_0}{2}\right)^2\right]. \tag{8}$$

Since $\bar{\eta}>0$, we get $t_{n,n\pm1}(R_0,\theta_0)<t_0$. Therefore, the main effect of explicitly considering the helical geometry is to reduce the strength of the π-π base coupling in the equilibrium configuration, as expected. Let us now relax the equilibrium structure, allowing for the propagation of low-frequency twist oscillations (acoustic modes), but keeping the radial variable describing H-bonding stretch oscillations fixed (no optical modes). In that case, Eq. (7) can be approximated as

$$t_{n,n\pm1}(R_0,\theta_{n,n\pm1}) \simeq t_0(1-\chi\theta_{n,n\pm1}^2), \tag{9}$$

for small enough twists, where the dimensionless parameter $\chi \equiv \bar{\eta}(R_0/l_0)^2>0$ measures the coupling strength between the charge and the lattice system. This expression generalizes the hopping function adopted in previous works,[18,20,21,31,32] which implicitly assumed $\chi=1/2$ (i.e., $t_{n,n\pm1}\simeq t_0\cos\theta_{n,n\pm1}$) for one-dimensional chains. As a matter of fact one usually gets $\chi>1$ in realistic conditions. For instance, making use of the values $\eta_{pp\pi}=-2.26$ and $\eta_{pp\sigma}=+5.27$ reported in Ref. 30 one obtains $\chi=2.92$. Albeit its approximate nature Eq. (9) reasonably reproduces the main features of the transfer integral versus twist angle dependence derived from detailed quantum-chemistry calculations,[24] as it is illustrated in Fig. 2.

Plugging Eq. (9) into Eq. (4) we obtain the following nearest-neighbor tight-binding equation of motion:

$$(E-\alpha_n(E))\psi_n - t_0(1-\chi\theta_{n,n+1}^2)\psi_{n+1} - t_0(1-\chi\theta_{n,n-1}^2)\psi_{n-1} = 0, \tag{10}$$

where ψ_n is the electronic wave function at site n. This expression generalizes the equation of motion usually considered within the framework of the Su-Schrieffer-Heeger Hamiltonian,[34] including the quadratic dependence $\theta_{n,n\pm1}^2$ in the off-diagonal terms (instead of a linear one). Thus, nonlinearity emerges in Eq. (10) as a natural consequence of the 3D DNA geometry.

III. HELICOIDAL EFFECTS

At very low temperatures the bases remain very close to the equilibrium positions, hence providing a suitable physical scenario to estimate the main contribution of geometrical (helical) effects on the charge transport. In that case, we can reasonably assume $\theta_{n,n+1}=\theta_0\,\forall n$, so that Eq. (10) reduces to

$$(E-\alpha_n(E))\psi_n - \tau_0(\psi_{n+1}+\psi_{n-1}) = 0, \tag{11}$$

where $\tau_0 \equiv t_0(1-\chi\theta_0^2)$. In the case of homopolymer chains, such as polyG-polyC or polyA-polyT, all the on-site energies are equal. Assuming periodic boundary conditions the dispersion relation can be expressed as $E=\alpha(E)+2\tau_0\cos(ql_0)$. This expression has the typical form for a monatomic chain, though in this case the renormalized on-site energy $\alpha(E)$ explicitly depends on the charge carrier energy according to Eq. (5). The energy spectrum consists of two asymmetric bands of width

$$W_\pm = \frac{\sqrt{\Delta_\pm}-\sqrt{\Delta_\mp}-4\tau_0}{2(\alpha_1-1)}, \tag{12}$$

separated by a gap of width

$$\Delta_g = \frac{4\tau_0-\sqrt{\Delta_+}-\sqrt{\Delta_-}}{2(\alpha_1-1)}, \tag{13}$$

where $\Delta_\pm=(a_0\pm2\tau_0)^2-8(\alpha_1-1)t^2+\gamma(\gamma-2a_0\mp4\tau_0)$.[15] By inspecting Eqs. (12) and (13) one realizes that the overall electronic structure depends on several physical mechanisms, including the aromatic base stacking between neighboring bp's, whose value depends on the helicoidal structure in terms of the parameter τ_0. In order to get a basic understanding on the physical significance of helicoidal effects we will adopt the values previously considered in the planar model discussed in Ref. 14, i.e., $\varepsilon_G=\varepsilon_C=t_{GC}\equiv0$, and $\gamma\equiv0$. In this case the energy spectrum exhibits two symmetric bands of width $W=2t_0|1-\chi\theta_0^2|$ separated by a gap of width $\Delta_g=2\sqrt{t_0^2(1-\chi\theta_0^2)^2+2t^2}-W$. Thus, helicoidal geometry produces two main effects in the electronic structure of DNA: (i) the highest occupied molecular orbital (HOMO) and lowest unoccupied molecular orbital (LUMO) bandwidths shrink, and (ii) the width of the gap increases with respect to the values obtained for planar models. Both changes degrade charge transport efficiency.

In order to analyze the role of helical effects we will compare the present helical model with the planar model previously discussed in Ref. 15. To this end, it is convenient

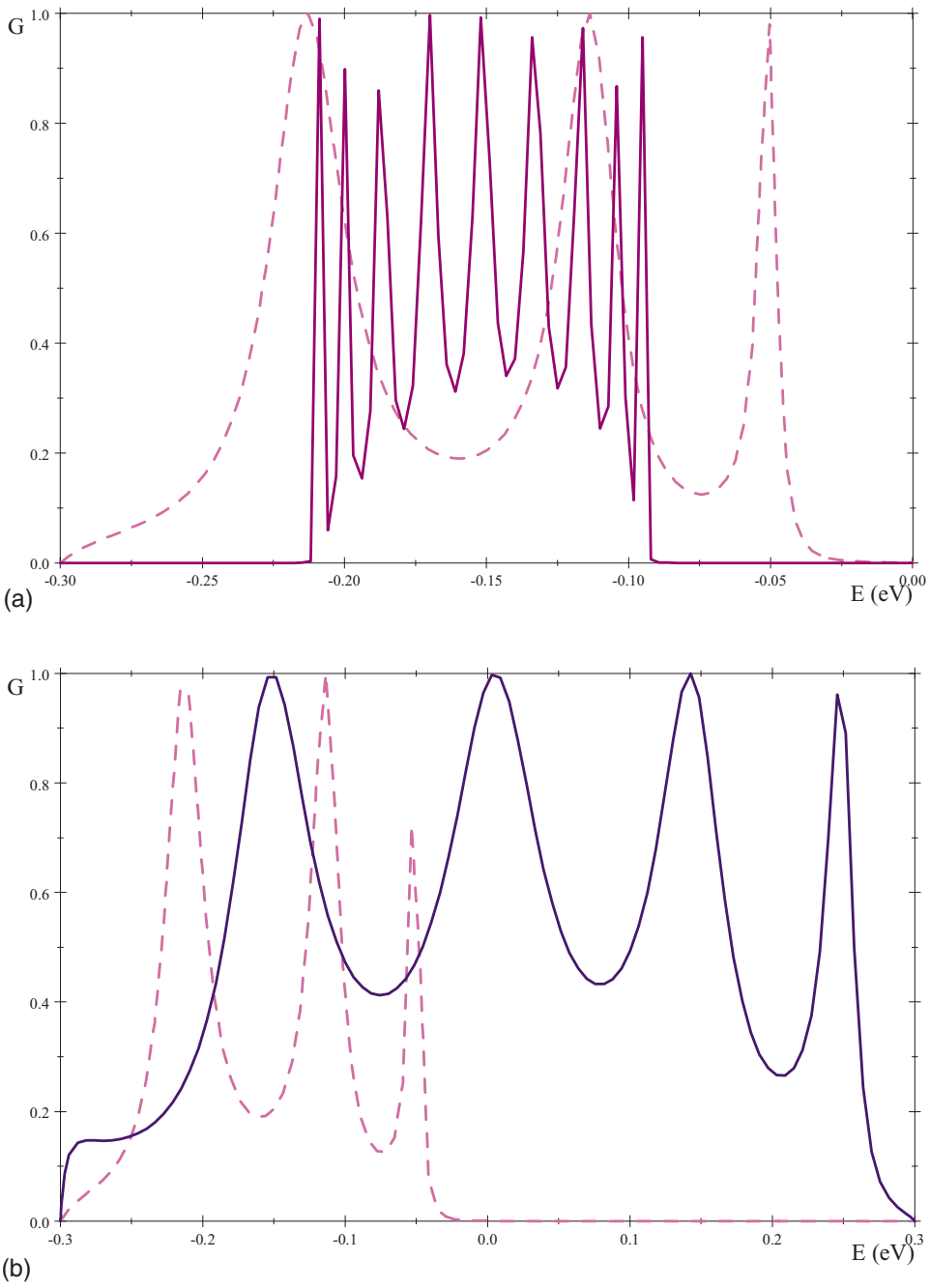

FIG. 3. (Color online). The Landauer conductance (in G_0 units) as a function of the Fermi level energy of a polyG-polyC oligomer with $N=10$ bp's corresponding to the planar model (gray curve) is compared to (a) that corresponding to the helicoidal model at the equilibrium configuration, and (b) that corresponding to a 3D model coupled to the ω_+ normal mode. The model parameters are $\varepsilon_A=8.25$ eV, $\varepsilon_T=9.13$ eV, $\varepsilon_G=7.77$ eV, $\varepsilon_C=8.87$ eV, $t_{GC}=0.90$ eV, $t_{AT}=0.34$ eV (Ref. 33), $t=1.5$ eV (Ref. 9), $t_0=0.15$ eV, $\gamma=12.27$ eV, and $\tau=t_M=0.15$ eV (Ref. 16). The origin of energy is set at ε_G.

to adopt the same model parameter values in both cases. Otherwise, it is difficult to determine to what extent the obtained differences are due to dimensional effects or to parameters change [for a detailed discussion of the adopted model parameters, see Sec. IV A in Ref. 16(b)]. In the absence of any applied voltage the fraction of tunneling electrons transmitted through a DNA chain of length N is given by the energy-dependent transmission coefficient $T_N(E)$, which is related to the Landauer conductance $G(E)=G_0T_N(E)$, where $G_0\equiv 2e^2/h\simeq 12\,906^{-1}\ \Omega^{-1}$ is the conductance quantum. The transmission coefficient can be obtained from the knowledge of the lead dispersion relation and the matrix elements of the metal-DNA-metal transfer matrix.[15,16] In Fig. 3(a), we compare the Landauer conductance corresponding to the helicoidal and planar models. As we see, the net effect of introducing helical structure is to reduce the conductance spectral width as compared to the value obtained for $\theta_0=0$.

IV. DYNAMICAL EFFECTS

The equations of motion, derived from Eq. (6) via the canonical equations, read

$$\ddot{\varphi}_n=\frac{k}{2m\xi^2}\left\{\left(1-\frac{l_0}{d_{n,n+1}}\right)f_{n+1}(\theta)-\left(1-\frac{l_0}{d_{n,n-1}}\right)f_{n-1}(\theta)\right\}, \tag{14}$$

where $f_{n\pm1}(\theta)\equiv c^2\theta_{n,n\pm1}+R_0^2\sin\theta_{n,n\pm1}$. The low-frequency response is obtained linearizing Eq. (14) by considering only linear terms of the Taylor expansion to obtain $\ddot{\varphi}_n\simeq\omega_0^2(\varphi_{n+1}$

$+\varphi_{n-1}-2\varphi_n)$, where $\omega_0 \equiv \sqrt{k/(2m)}$ is the natural twist frequency of each bp. The corresponding dynamical equation for the variables $\theta_{n,n\pm1}$ is then straightforwardly derived to get

$$\ddot{\theta}_{n,n+1} - \ddot{\theta}_{n,n-1} = \omega_0^2(\theta_{n+1,n+2} - 3\theta_{n,n+1} + 3\theta_{n,n-1} - \theta_{n-1,n-2}). \tag{15}$$

This expression describes a *correlated* motion involving three consecutive bp's (codon unit cell). Searching for solutions in the form of linear waves we plug the ansatz $\theta_{n,m} = Ae^{i\omega t}\cos[(n+m)q/2]$, where q is the wave number, into Eq. (15) to obtain the dispersion relation $\omega^2 = 4\omega_0^2 \sin^2(q/2)$, which agrees with that reported in Ref. 26. Finally, inserting $\theta_{n,m}$ into Eq. (10) we get

$$(E - \alpha_n)\psi_n - \tau_0(\psi_{n+1} + \psi_{n-1}) + B[\psi_{n+1}\cos(2n+1)q + \psi_{n-1}\cos(2n-1)q] = 0, \tag{16}$$

where $B \equiv t_0\chi\theta_0^2$, and we have chosen $A = \sqrt{2}\theta_0$. This expression properly extends Eq. (11) by including charge-lattice interaction effects. From the dispersion relation we have $q = \cos^{-1}\Omega$, where we have introduced the auxiliary variable $\Omega \equiv 1 - \omega^2/2\omega_0^2$ ($\Omega \in [-1,1]$). Thus, we can express Eq. (16) in the form

$$(E - \alpha_n(E))\psi_n - \tau_0(\psi_{n+1} + \psi_{n-1}) + B(\psi_{n+1}T_{2n+1}(\Omega) + \psi_{n-1}T_{2n-1}(\Omega)) = 0, \tag{17}$$

where $T_k(\Omega) \equiv \cos(k\cos^{-1}\Omega)$ are Chebyshev polynomials of the first kind. Making use of the multiplication formula $T_{k+l} = T_kT_l - (1-\Omega^2)U_{k-1}U_{l-1}$, where $U_{k-1}(\Omega)$ are Chebyshev polynomials of the second kind, and taking into account the relationships $T_{\pm1}(\Omega) = \Omega$, $U_0(\Omega) = 1$, and $U_{-2}(\Omega) = -1$, we can express Eq. (17) in the form

$$(E - \alpha_n(E))\psi_n - (\tau_0 - B\Omega T_{2n})(\psi_{n+1} + \psi_{n-1}) + B(1-\Omega^2)U_{2n-1}(\psi_{n-1} - \psi_{n+1}) = 0. \tag{18}$$

Introducing the auxiliary parameter $\tilde{\Omega} \equiv 2\Omega^2 - 1$ ($\tilde{\Omega} \in [-1,1]$), and making use of the functional equations $T_{2k}(\Omega) = T_k(2\Omega^2-1)$ and $U_{2k-1}(\Omega) = 2\Omega U_{k-1}(2\Omega^2-1)$, we finally obtain

$$(E - \alpha_n)\psi_n - (\tau_0 - B\Omega T_n(\tilde{\Omega}))(\psi_{n+1} + \psi_{n-1}) + 2B\Omega(1-\Omega^2)U_{n-1}(\tilde{\Omega})(\psi_{n-1} - \psi_{n+1}) = 0. \tag{19}$$

By inspecting Eq. (19) we realize that the motion equation considerably simplifies in the cases $\Omega = 0$ and $\Omega = \pm 1$. In the case $\Omega = 0$ (i.e., $\tilde{\Omega} = -1$, $\omega = \sqrt{2}\omega_0$), Eq. (19) reduces to Eq. (11). In this way, when a charge couples to the $q = \pi/2$ vibrational state the resulting charge dynamics mimics that corresponding to the equilibrium configuration one. The frequencies corresponding to the cases $\Omega = \pm 1$ (i.e., $\tilde{\Omega} = 1$) are located at the edges of the frequency spectrum ($\omega_+ = 0$ and $\omega_- = 2\omega_0$). Then, using the relationship $T_n(1) = 1, \forall n$, Eq. (19) takes the form

$$(E - \alpha_n(E))\psi_n - \tau_\pm(\psi_{n+1} + \psi_{n-1}) = 0, \tag{20}$$

where $\tau_+ = t_0(1 - 2\chi\theta_0^2)$ and $\tau_- = t_0$ are, respectively, labeled after frequencies $\omega_\pm$. The mathematical structure of Eq. (20) describes a charge propagating through a linear chain with an effective transfer integral whose value depends on the considered frequency. We note that, broadly speaking, an increase in the transfer integral value usually contributes to a lowering of the system energy [see Eq. (4)] so that the charge gets localized by its interaction with the lattice (polaronic effect).[34–36] In the ω_+ case, however, the transfer integral becomes negative ($\tau_+ = -1.3t_0 \simeq -0.2$ eV) and charge becomes delocalized instead. The normal modes corresponding to the DNA codon shown in Fig. 1(a) are $\omega_1 = 0 = \omega_+$, $\omega_2 = \sqrt{2}\eta\omega_0$, and $\omega_3 = \sqrt{6}\eta\omega_0$, where $\eta \equiv f(\theta_0)l_0^{-1}\xi^{-1} \simeq 0.961$. Therefore, the lowest-frequency state ω_+ is a normal mode

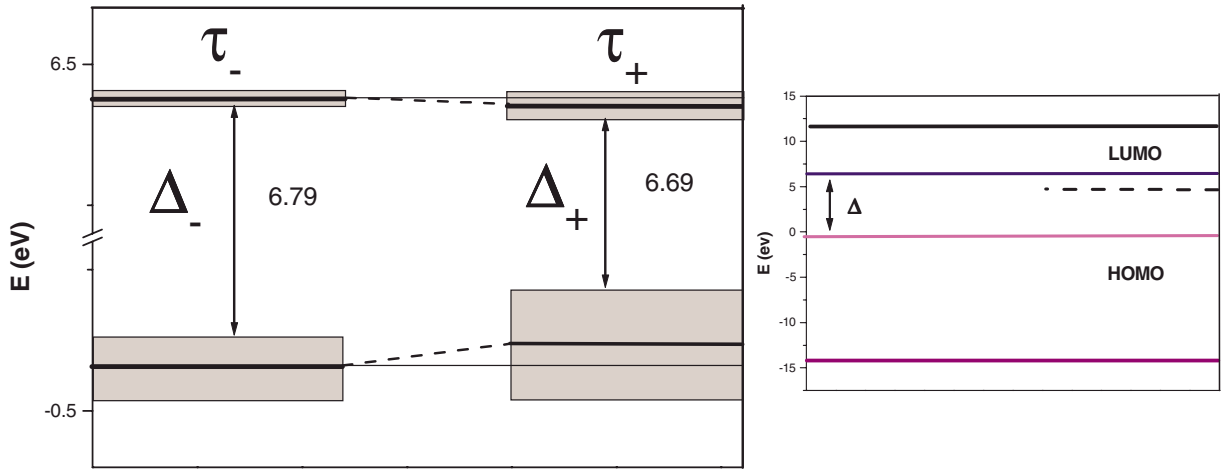

FIG. 4. (Color online) HOMO-LUMO bands for a polyGACT-polyCTGA chain corresponding to the vibrational states ω_- and ω_+ (left panel). The overall electronic spectrum structure is shown in the right panel on a broader energy scale. The spectra have been derived from Eq. (20) making use of the same model parameters used to plot Fig. 3.

TABLE I. Allowed band locations (E_i), bandwidths (W_i), and gap widths (Δ_{ij}) in the energy spectrum of an effective polyGACT-polyCTGA chain with a charge coupled to the $\omega_\pm$ vibration states.

Band center (eV)	ω_-	ω_+	Band width (meV)	ω_-	ω_+	Gap width (eV)	ω_-	ω_+
E_1	−14.209	−14.229	W_1	269	451			
E_2	−0.423	−0.383	W_2	120	200	Δ_{12}	13.591	13.590
E_3	+6.440	+6.430	W_3	29	48	Δ	6.788	6.689
E_4	+11.595	+11.656	W_4	177	300	Δ_{34}	5.052	5.052

describing the simultaneous rotation of all bp's around the helical axis by an arbitrary amount. Since H_l is invariant under the transformation $\varphi_n' \rightarrow \varphi_n + \epsilon$, this collective movement can be regarded as a Goldstone mode arising from the presence of a discrete arrangement of bp's along the DNA backbone (breaking the continuous symmetry proper of a uniform helical string). On the other hand, the coupling of the charge to the ω_- vibration state results in a competition between dynamical and helicoidal effects, so that the equation of motion reduces to that of an effective two-dimensional model in this case.

For a periodic distribution of on-site energies, Eq. (20) is formally identical to the polyGACT-polyCTGA DNA chain studied in Ref. 16 by simply replacing $t_0 \rightarrow \tau_\pm$. Thus, the electronic dispersion relation can be written as $4\tau_\pm^2 \cos^2(ql_0) = E^2 - (\alpha+\beta)E + \alpha\beta$. The energy spectra corresponding to the effective hoping $\tau_\pm$ are shown in Fig. 4. The location of the different allowed bands and their respective bandwidths are listed in Table I. By comparing both spectra two main features can be observed close to the Fermi level: (i) a significant broadening of the bandwidths, and (ii) a narrowing of the HOMO-LUMO gap width for the ω_+ spectrum as compared to the ω_- one. Therefore, the coupling with the low band edge vibrational state results in a *significant improvement* of the charge transport efficiency through the DNA chain, as it is illustrated by the broadening of the Landauer conductance spectral window shown in Fig. 3(b). A similar broadening effect has been reported for polyA-polyT chains with 15 bp's as arising from compressional acoustic modes propagating through the helical axis (although in the case of a polyG-polyC chain of the same length a narrowing effect was observed instead).[37]

Landauer conductance is a useful magnitude in the context of molecular electronics, which allows for a direct comparison with experimental current-voltage curves.[14] In fact, one expects the energy interval under the $T(E)$ curve to be proportional to the electrical current flowing through the molecule.[38] Nonetheless, the conductance values shown in Fig. 3 cannot be directly compared with experimental values obtained for short DNA chains (ranging within the interval $G = 10^{-3} - 10^{-6} G_0$), since those experiments are performed at room temperatures.[37,39] From basic physical principles one expects the acoustic modes will significantly affect the conductance at temperatures below the Debye temperature, which measures the temperature above which all modes begin to be excited, and below which modes begin to be progressively inactive. By assuming a speed of sound in B-DNA form of 1900 ms^{-1},[40] and a lattice constant of approximately 0.34 nm, the Debye temperature was estimated as $\Theta_D \simeq 166$ K for longitudinal compression modes.[37] On the other hand, specific heat measurements of biological DNA samples over the temperature range 0.5–5 K suggest significant smaller values ($\Theta_D \simeq 20-40$ K) for torsional modes.[41] Accordingly, we conclude that the coupling effect predicted in our work would require low temperature measurements of the DNA electrical conductance to be clearly appreciated.

V. CONCLUSIONS

In this work we consider the interplay between the helical structure and low-frequency dynamics of DNA bp's and their mutual influence on charge transfer efficiency. To this end, we have expressed charge-lattice interaction in terms of nearest-neighbor tight-binding equations describing the propagation of the charge through an effective linear lattice for certain frequency values. The corresponding effective hopping terms include both helicoidal and dynamical effects in an intertwined fashion, allowing for a unified treatment of charge-lattice coupled dynamics in a fully analytical way in terms of Chebyshev polynomials. In this way, we disclose a number of remarkable symmetries of the motion equations themselves, which may be implemented with accurate charge transfer parameters derived from quantum chemistry and molecular dynamics approaches in a straightforward way.[42] Although an ensemble of bp's twisting back and forth around the helix axis generally results in a degraded charge transfer efficiency, a significant improvement of charge migration can occur via charge coupling to the lattice Goldstone mode. This fundamental mechanism is expected to occur in other π-π molecular wires in the low temperature limit as well.[43] In this regard, our work complements those previous works where the structural fluctuations of the DNA double helix are described by sampling the initial angular velocities and twist angles from a Boltzmann distribution at room temperature. In comparison, in the present study one focuses on low-frequency normal mode propagation (as opposed to incoherent thermal fluctuations), which are expected to dominate the molecule dynamics in the limit of very low temperatures (rather than room temperature ones).

ACKNOWLEDGMENTS

I warmly thank Alexander Voityuk for useful comments. I acknowledge M. V. Hernández for a critical reading of the manuscript. This work has been supported by the Universidad Complutense de Madrid through Project No. PR27/05-14014-BSCH.

[1] R. G. Endres, D. L. Cox, and R. R. P. Singh, Rev. Mod. Phys. **76**, 195 (2004).
[2] C. R. Treadway, M. G. Hill, and J. F. Barton, Chem. Phys. **281**, 409 (2002).
[3] E. B. Starikov, Philos. Mag. **85**, 3435 (2005); Phys. Chem. Chem. Phys. **4**, 4523 (2002).
[4] M. Taniguchi and T. Kawai, Phys. Rev. E **70**, 011913 (2004).
[5] J. P. Lewis, Th. E. Cheatham III, E. B. Starikov, H. Wang, and O. F. Sankey, J. Phys. Chem. B **107**, 2581 (2003).
[6] E. Artacho, M. Machado, D. Sánchez-Portal, P. Ordejón, and J. M. Soler, Mol. Phys. **101**, 1587 (2003).
[7] P. J. de Pablo, F. Moreno-Herrero, J. Colchero, J. Gomez Herrero, P. Herrero, A. M. Baro, P. Ordejón, J. M. Soler, and E. Artacho, Phys. Rev. Lett. **85**, 4992 (2000).
[8] G. Cuniberti, E. Maciá, A. Rodríguez, and R. A. Römer, in *Charge Migration in DNA: Physics, Chemistry and Biology Perspectives*, edited by T. Chakraborty (Springer, Berlin, 2007).
[9] K. Iguchi, Int. J. Mod. Phys. B **18**, 1845 (2004); J. Phys. Soc. Jpn. **70**, 593 (2001); Int. J. Mod. Phys. B **11**, 2405 (1997).
[10] D. Klotsa, R. A. Römer, and M. S. Turner, Biophys. J. **89**, 2187 (2005).
[11] X. F. Wang and T. Chakraborty, Phys. Rev. Lett. **97**, 106602 (2006).
[12] R. A. Caetano and P. A. Schulz, Phys. Rev. Lett. **95**, 126601 (2005); **96**, 059704 (2006); A. Sedrakyan and F. Domínguez-Adame, *ibid.* **96**, 059703 (2006).
[13] E. Díaz, A. Sedrakyan, D. Sedrakyan, and F. Domínguez-Adame, Phys. Rev. B **75**, 014201 (2007).
[14] G. Cuniberti, L. Craco, D. Porath, and C. Dekker, Phys. Rev. B **65**, 241314(R) (2002).
[15] E. Maciá and S. Roche, Nanotechnology **17**, 3002 (2006).
[16] (a) E. Maciá, Phys. Rev. B **74**, 245105 (2006); (b) **75**, 035130 (2007).
[17] A. A. Voityuk, J. Jortner, M. Bixon, and N. Rösch, J. Chem. Phys. **114**, 5614 (2001).
[18] S. Roche, Phys. Rev. Lett. **91**, 108101 (2003).
[19] Y. Zhu, C. C. Kaun, and H. Guo, Phys. Rev. B **69**, 245112 (2004).
[20] W. Ren, J. Wang, Z. Ma, and H. Guo, Phys. Rev. B **72**, 035456 (2005); J. Chem. Phys. **125**, 164704 (2006).
[21] A.-M. Guo and H. Xu, Physica B **391**, 292 (2007).
[22] R. Gutiérrez, S. Mandal, and G. Cuniberti, Phys. Rev. B **71**, 235116 (2005).
[23] R. Gutiérrez, S. Mohapatra, H. Cohen, D. Porath, and G. Cuniberti, Phys. Rev. B **74**, 235105 (2006).
[24] K. Senthilkumar, F. C. Grozema, C. Fonseca Guerra, F. M. Bickelhaupt, F. D. Lewis, Y. A. Berlin, M. A. Ratner, and L. A. Siebbeles, J. Am. Chem. Soc. **127**, 14894 (2005).
[25] M. Barbi, S. Cocco, and M. Peyrard, Phys. Lett. A **253**, 358 (1999).
[26] S. Cocco and R. Monasson, Phys. Rev. Lett. **83**, 5178 (1999); J. Chem. Phys. **112**, 10017 (2000).
[27] J. Agarwal and D. Hennig, Physica A **323**, 519 (2003).
[28] F. Palmero, J. F. R. Archilla, D. Hennig, and F. R. Romero, New J. Phys. **6**, 13 (2004).
[29] The role of higher-frequency H-bonding stretching modes was considered by H. Yamada, E. B. Starikov, D. Hennig, and J. F. R. Archilla, Eur. Phys. J. E **17**, 149 (2005); H. Yamada, E. B. Starikov, and D. Hennig, Eur. Phys. J. B **59**, 185 (2007).
[30] R. G. Endres, D. L. Cox, and R. R. P. Singh, arXiv:cond-mat/0201404 (unpublished).
[31] Z. G. Yu and X. Song, Phys. Rev. Lett. **86**, 6018 (2001).
[32] W. Zhang, A. O. Govorov, and S. E. Ulloa, Phys. Rev. B **66**, 060303(R) (2002).
[33] Y. J. Yan and H. Zhang, J. Theor. Comput. Chem. **1**, 225 (2002).
[34] E. M. Conwell and S. V. Rakhmanova, Proc. Natl. Acad. Sci. U.S.A. **97**, 4556 (2000).
[35] E. B. Starikov, Philos. Mag. Lett. **83**, 699 (2003).
[36] J. X. Zhu, K. Ø. Rasmussen, A. V. Balatsky, and A. R. Bishop, J. Phys.: Condens. Matter **19**, 136203 (2007).
[37] H. van Zalinge, D. J. Schiffrin, A. D. Bates, E. B. Starikov, W. Wenzel, and R. J. Nichols, Angew. Chem., Int. Ed. **45**, 5499 (2006).
[38] S. Datta, *Electronic Transport in Mesoscopic Systems* (Cambridge University Press, Cambridge, 1995).
[39] J. Hihath, F. Chen, P. Zhang, and N. Tao, J. Phys.: Condens. Matter **19**, 215202 (2007); B. Xu, P. Zhang, X. Li, and N. Tao, Nano Lett. **4**, 1105 (2004); J. Hihath, B. Xu, P. Zhang, and N. Tao, Proc. Natl. Acad. Sci. U.S.A. **102**, 16979 (2005).
[40] M. B. Hakim, S. M. Lindsay, and J. Powell, Biopolymers **23**, 1185 (1984).
[41] I. S. Yang and A. C. Anderson, Phys. Rev. B **35**, 9305 (1987).
[42] A. A. Voityuk, Chem. Phys. Lett. **439**, 162 (2007).
[43] R. Di Felice, A. Calzolari, and H. Zhang, Nanotechnology **15**, 1256 (2004).